GeoResJ 3-4 (2014) 9–18

Contents lists available at ScienceDirect

GeoResJ

journal homepage: www.elsevier.com/locate/GRJ

Effect of particle mixing morphology on aerosol scattering and absorption: A discrete dipole modeling study

Qing Zhang, J.E. Thompson *

Department of Chemistry and Biochemistry, MS1061, Texas Tech University, Lubbock, TX 79409-1061, United States

ARTICLE INFO

Article history:
Received 1 April 2014
Revised 27 June 2014
Accepted 5 July 2014
Available online 5 August 2014

Keywords:
Airborne particles
Light scattering
Visibility
Climate forcing
Mixing rule
Engulfed particles
Core-shell
Phase separated particles

ABSTRACT

Atmospheric aerosol particles may undergo phase separation due to differences in miscibility. This alters the morphology of particles such that they are no longer well-mixed, simple spheres. As a result, scattering and absorption of sunlight in Earth's atmosphere could be affected. In turn, this may alter direct climate forcing by aerosols. In this work we examine the impact of phase separation on aerosol optics for the bi-sphere, core–shell, and engulfed morphologies. We find bi-spherical particles often exhibit very different scattering and absorption cross-sections for a mid-visible wavelength (0.53 μm) relative to an equivalent, volume-weighted spherical case. Optical differences are largely driven by the particle shape, rather than differences in refractive index between phases. However, when averaged across a typical urban particle size distribution, the differences in light scattering largely vanish and bi-sphere and volume equivalent models generally agreed to within 10% for dielectric particles. For particles that are light absorbing, the bi-sphere and volume averaged cases often yielded dissimilar results with the volume-averaged case reflecting absorption >10% more than the phase separated particles. This was particularly true for bi-spheres in which one component particle is strongly light absorbing. Core–shell and engulfed morphologies yield volume scattering efficiencies within a few percent of volume-weighted spheres. However, modeled light absorption between the phase separated and volume averaged models frequently differ by >20% when inclusions absorb light strongly. Therefore, modeling light absorption of mixed-phase particles through the volume-mixing rule cannot be recommended.

Introduction

Recent research has discovered that airborne particles dispersed in Earth's atmosphere likely undergo phase separation driven by differences in solubility and molecular polarity [1–7]. Such internally mixed particles are often described as containing an 'organic' component and an inorganic or aqueous component that phase separate. The 'organic' phase is largely nondescript, being comprised of potentially hundreds of compounds. A fraction of the organic materials may be light absorbing compounds. The inorganic phase is often modeled as ammonium sulfate or ammonium nitrate as these materials have historically been present in atmospheric aerosol in significant quantities. For particles that do phase separate there are many possible morphologies, however, two specific models have emerged. First, a core–shell arrangement can result in which a spherical core of material is coated with a concentric shell of the phase-separated material. A second possibility has been termed 'engulfed' in which phase separated droplets form an interface of variable surface area at the droplet surfaces.

For this work, we consider several of the possible morphologies. One extreme morphology is when particle materials form two spheres (or near spheres) that touch on edge, but remain phase separated. Here, we model this type of particle as a true bi-sphere, in which droplets touch at a single point on their surface. We also consider core–shell morphology, and 'engulfed' particles in which a film of phase-separated material accumulates on the surface of the second solvent. Fig. 1 illustrates micrographs of several phase-separated particles that have appeared in previous literature along with sketches of the particle types and particle categories considered in this report.

Our laboratory has a strong interest in the measurement and modeling of aerosol optics [8–16]. Given the apparent inclination for materials in aerosols to phase separate, it is important to understand how this phase separation may influence optical properties of aerosols. Phase separated particles may exhibit additional interfaces of differing refractive index and/or increased surface area relative to homogeneous particles. As a result, the light

* Corresponding author.
E-mail address: jon.thompson@ttu.edu (J.E. Thompson).

http://dx.doi.org/10.1016/j.grj.2014.07.001
2214-2428/

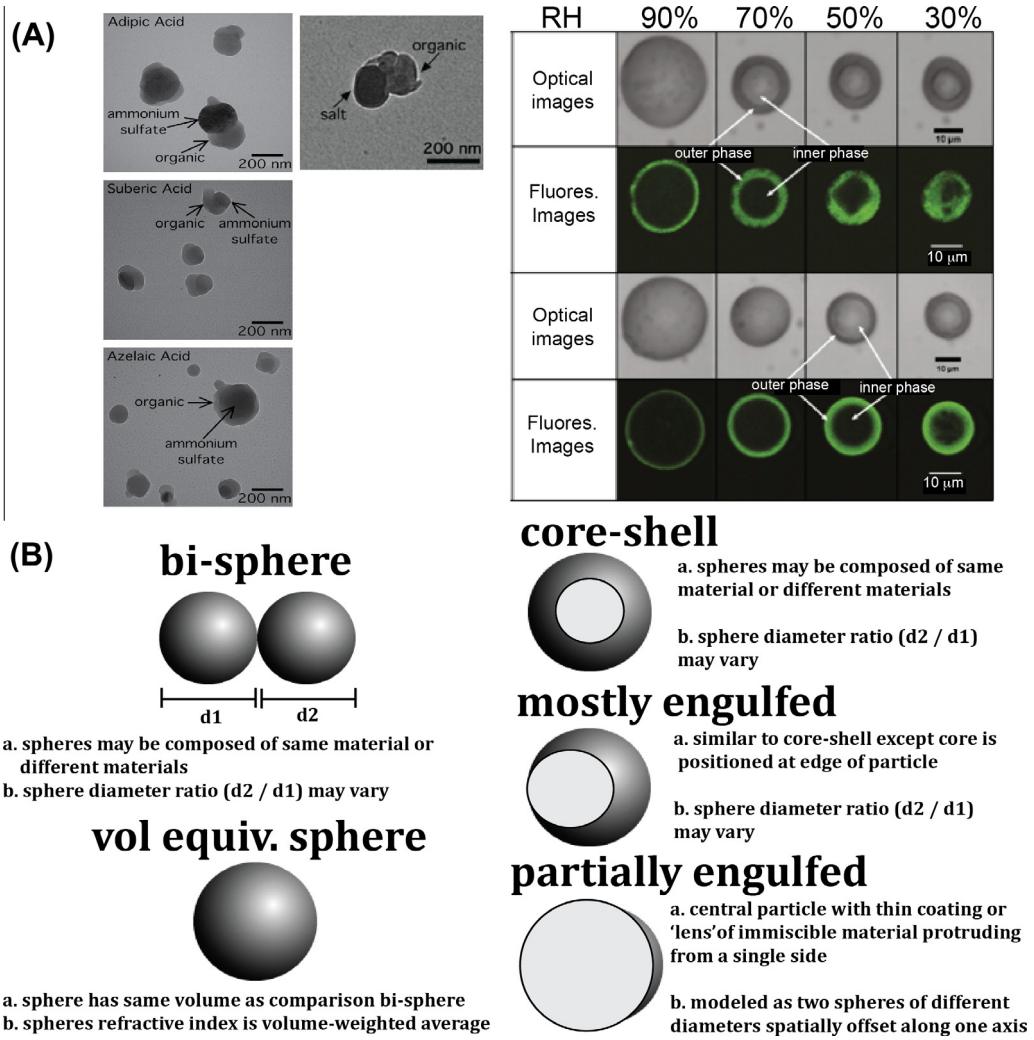

Fig. 1. (A) Micrographs from previous literature providing evidence for phase separation within atmospheric particulate matter. Micrographs are reprinted with permission from *Proc. Nat Acad Sci* 2012;109(33):13188–13193, *Anal Chem* 2014;86(5):2436–2442, and *J Am Chem Soc* 2013;135(43):16046–16049. The latter two figures are copyright American Chemical Society. (B) Particle models used for the discrete dipole modeling in this work. For the bi-sphere, core–shell, mostly engulfed, and partially engulfed cases the individual sphere diameters and refractive indices were varied.

scattering and absorption properties of the aerosol may be altered because of the biphasic behavior. In essence, the phase separation may cause increased or decreased scattering and absorption. Because aerosol scattering and absorption is believed to affect Earth's climate through direct radiative forcing, understanding the effect of phase separation upon radiative transfer is an important goal.

Lang-Yona et al. [17] have previously investigated core–shell geometries, but to the best of our knowledge this manuscript is one of the first to consider bi-spherical and engulfed geometries caused by phase separation. Here, we use a publically available discrete dipole code (ADDA) [18] to model light scattering and absorption for various phase-separated particles and compare results to volume-averaged equivalent spheres. We carefully constrain the modeling experiments to maintain constant particle volume for the comparison test cases, but simply distribute the volume amongst different shapes. Again, Fig. 1 presents explanatory drawings of each case along with micrographs that inspire each model. The micrographs have all appeared in previous literature. We constrain refractive indices used to reflect authentic aerosol components as much as possible.

Methods

Discrete-dipole modeling

Determination of light scattering and absorption cross-sections (C_{scat} or C_{abs}; μm^2) for individual particles were accomplished through the Amsterdam Discrete Dipole Approximation code [18] (ADDA) downloaded from https://code.google.com/p/a-dda/. This code allows the user to adjust the diameters and refractive index for each sphere independently. For this work, a wavelength of 0.53 microns was always used. Since the optical effects for particles may depend upon their orientation with respect to the incident light beam, averaging optical results for many orientations of the particle is required. The ADDA program treats this problem by sequentially varying three Euler angles (α, β, γ) that define the particles orientation with respect to the incident beam. Alpha was modified from 0° to 360° in 32 steps, beta from 0° to 180° in up to 17 steps, and gamma from 0° to 360° in up to 16 steps. Therefore, the optical cross sections and S_{11} element of the scattering matrix we report for bi-spheres represent values averaged over many orientations. The accuracy of discrete dipole computations

depends upon maintaining a high enough density of dipoles within the scattering particle. For this work, we used the ADDA default setting that provides, at minimum, 10 dipoles per wavelength, per spatial dimension, inside the scattering particle. The exact dipole density varied between runs but was always >16 dipoles per wavelength. For particles with diameters of $<\lambda/2$, ADDA often used >50 dipoles per λ. The number of dipoles used per spatial dimension was similar to accurate results reported in previous literature [19,20]. In addition, direct comparison of light scattering cross sections obtained from ADDA with exact Mie solutions for spheres of $m = 1.53$ always yielded agreement to within 2% for 23 tested diameters between 20 nm and 1.5 μm. It appears as if the default dipole density used is effective to reproduce light scattering for spherical geometries. Bisphere particles were generated in ADDA using the Biellipsoid particle shape. The "coated" particle shape was used to model core–shell and mostly engulfed particles. Partially engulfed particles were modeled using a user defined particle shape file. This shape file was generated by combining two spheres of varying diameter. One sphere was translated by 25% of the particle diameter in the x-dimension. Then, any points within the shifted sphere that still reside in the volume of the first sphere were deleted. This assures one intact sphere is present (sphere 1) and a thin coating layer is present on a fraction of the spheres area.

The refractive index of volume-weighted equivalent spheres was determined by linearly averaging the real and imaginary portion of refractive indices of component materials weighted by the volume of each component. For example, a bi-sphere composed of two spheres with equivalent diameters and refractive indices of $m = 1.\ 63 + 0.02i$ and $m = 1.53 + 0i$ would result in a volume weighted refractive index of $m = 1.58 + 0.01i$. This mixing rule is the simplest of a variety of options previously reported in the literature [21–25]. This mixing rule was always used to generate the volume equivalent sphere test cases, and is referred to as the 'volume-mixing rule.'

The differential scattering cross section can be computed by extracting the S_{11} element from the scattering matrix and dividing by k^2 according to Bohren and Huffman [26]:

$$\frac{dC_{\text{scat}}}{d\Omega} = \frac{S_{11}}{k^2}$$

where

$$k = \frac{2\pi m}{\lambda}$$

In this equation, m is the refractive index and λ is wavelength. The phase function of scattering (P) is the differential scattering cross section divided by the scattering cross section integrated over all angles (C_{scat}):

$$P(\theta) = \frac{1}{C_{\text{scat}}}\frac{dC_{\text{scat}}}{d\Omega}$$

The asymmetry parameter (g) is defined as the intensity weighted average of the cosine of scattering angle [27] by

$$g = \frac{1}{2}\int_0^{\pi} \cos\theta\ P(\theta)\sin\theta\ d\theta$$

and backscatter fraction (b) computed by simply setting proper limits of integration:

$$b = \frac{\int_{\pi/2}^{\pi} P(\theta)\sin\theta\ d\theta}{\int_0^{\pi} P(\theta)\sin\theta\ d\theta}$$

For this work, we determined the asymmetry parameter (g) directly using ADDA. For bi-spheres, the asymmetry parameter will change with particle orientation with respect to the beam. We have simply averaged the asymmetry parameter for 12 random orientations for each bi-sphere considered. Um and McFarquhar have previously averaged asymmetry parameter (g) obtained from ADDA over many particle orientations for the study of ice crystals [28]. Estimation of the backscatter fraction (b) was accomplished using the polynomial suggested by Marshall et al. and the value for asymmetry parameter obtained from ADDA [27].

Analysis of resultant ADDA data and reconstruction of integrated optical properties

Optical cross-sections obtained were converted to a volume-based scattering or absorption efficiency (ϕ_{scat} or ϕ_{abs}) by dividing by the scattering particle's volume (mL), i.e.

$$\phi_{\text{scat}} = \frac{C_{\text{scat}}}{\text{particle volume (mL)}}$$

$$\phi_{\text{abs}} = \frac{C_{\text{abs}}}{\text{particle volume (mL)}}$$

These efficiency parameters allow easy consideration of the quantity of light absorbed or scattered on a per-material basis regardless of particle shape. In this work we report this variable in units of m^2/mL. Note, this volume scattering and absorption efficiency is not equivalent to single particle scattering and absorption efficiency parameters (so-called Q terms) commonly discussed in light scattering circles.

To better understand the possible effects of partitioning into bi-spheres, we have worked to reconstruct the scattering and absorption coefficient (m^{-1}) for a typical urban aerosol. For this reconstruction, we fit a log – normal distribution to the volume concentration data reported by Zhou et al. [29] collected in Pittsburgh (means are reported within Table 2 of the reference). This fit yielded the following equation:

$$y = 0.523 + 31.23\exp\left[-\left(\frac{\ln\left(\frac{x}{0.346}\right)}{0.7868}\right)^2\right]$$

Here x is the particle diameter in micrometers, and the y-variable $dN_v/d\log Dp$ ($\mu m^3/cm^3$). This equation was then used along with the ϕ_{scat} and ϕ_{abs} data from ADDA analysis to numerically integrate across the modeled size distribution for particles between 20 nm and 1.5 μm diameter. This reconstruction considers the extremes of phase partitioning for all material present in the hypothetical sample. In effect, either 100% volume equivalent spheres, or 100% bi-sphere geometry. We have intentionally chosen these extreme cases to better understand the absolute limits of the phase partitioning effect. The reconstructed results should never be considered an average, or representative case.

Results and discussion

Effect of bi-sphere geometry on scattering for homogeneous dielectric particles

Fig. 2A illustrates a comparison between light scattering efficiency (ϕ_{scat}) for spherical particles and bi-spheres for particles with $m = 1.53 + 0i$. Here, we define scattering efficiency as the ratio of scattering cross – section (C_{scat}, m^2) divided by particle volume (mL). Therefore, this variable expresses the efficiency with which light is scattered on a per-volume basis. This allows direct comparison between different particle morphologies. In addition, the bi-sphere geometry considered in Fig. 2A features two identical particles (both diameter and composition). The particle volume reflects the sum of both spheres.

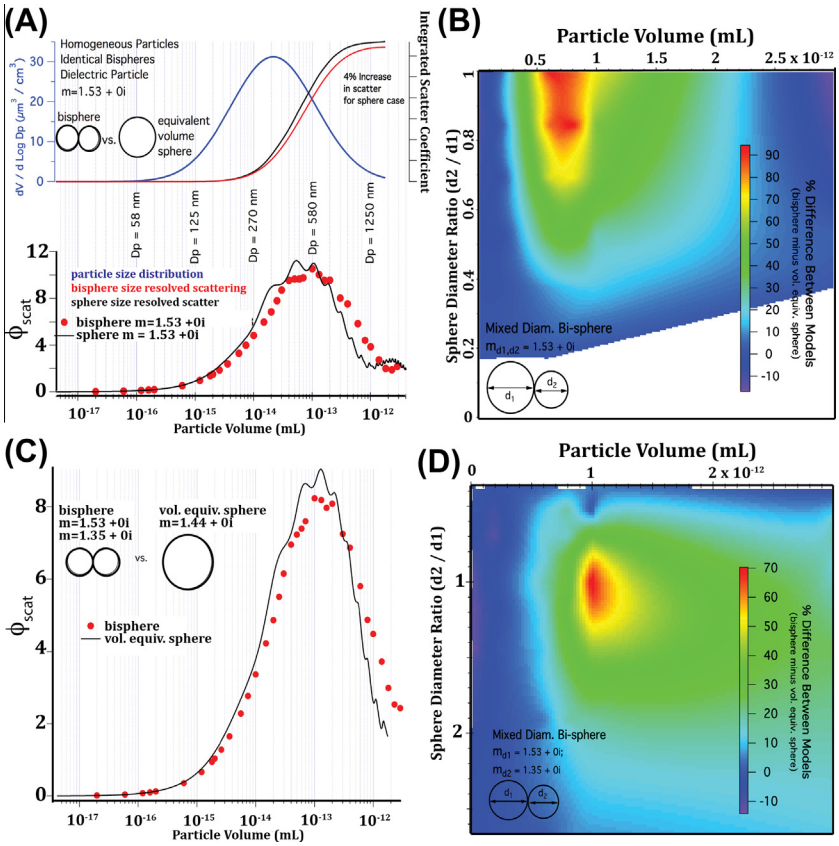

Fig. 2. Comparison of light scattering efficiencies (ϕ_{scat}) for bi-sphere and equivalent volume spheres for dielectric particles. (A) Red and black traces show reconstructed aerosol scattering coefficient (m^{-1}) for the bi-sphere and equivalent sphere cases. The blue trace is the size distribution used to generate the data adapted from Ref. [29]. Plots of single particle scattering cross-section (m^2) normalized to particle volume vs. particle volume (mL) for the bi-sphere (●) and equivalent sphere (—) cases when $m = 1.53 + 0i$ and $d_2 = d_1$. (B) Image plot depicting the percent difference in single particle scattering cross-section between bi-sphere and volume equivalent sphere cases as a function of total particle volume and bi-sphere diameter ratio. (C) Plot of volume normalized scattering efficiency (ϕ_{scat}) vs. particle volume for bi-spheres with $m = 1.53 + 0i$ and $1.35 + 0i$ and a volume averaged sphere of $m = 1.44 + 0i$. (D) Image plot similar to B but for spheres of different refractive index. For this diagram, sphere diameter ratios <1 were also explored since bi-sphere refractive indices differ. Largest difference between the models occurs when particle volume is near 1 femtoliter and bi-sphere diameter ratio near 1. (For interpretation of the references to colour in this figure legend, the reader is referred to the web version of this article.)

As observed in the figure the function goes through a maximum for particles of a few hundred nanometers diameter (roughly 10^{-13} cm^3 volume) and then becomes smaller before leveling off around a volume of 1×10^{-12} cm^3. For very small particles in the Rayleigh scattering regime, particle shape is not an important factor. Rather, scattering cross sections scale with the number of scattering entities (here molecules) oscillating in-phase. Consequently, little difference is observed between spherical and bi-spherical particles. As the particle volume increases, the plot for bi-spherical geometry (red circles) appears shifted to the right compared to the equivalent sphere case illustrated by the solid black line. This shift is easy to explain from a physical perspective if we invoke a model in which the bi-spheres act largely as independent scatterers. Here, the bi-sphere geometry supports the existence of two identical spheres, both with dimensions that maximize Mie scattering efficiency, while doubling the total particle volume. The volume scattering efficiency (ϕ_{scat}) of bi-spheres does not reach the maximum observed for a single sphere. While Fig. 2A illustrates results for $m = 1.53$, use of a lower refractive index ($m = 1.44$) for equivalent diameter spheres yielded a similar shift in the efficiency compared to the equivalent sphere case. As such, this shift to larger volume particles appears to be driven by the geometry of the particle rather than refractive index.

Fig. 2B further supports the argument that distributing particle volume as a bi-sphere is the driving force behind observed differences. In Fig. 2B, we plot the percent difference in scattering cross-section (C_{scat}) between the bi-sphere and volume equivalent sphere cases (bi-sphere – vol. equiv. sphere/vol. equiv. sphere) as a function of sphere diameter ratio (d_2/d_1) and total particle volume. As observed, the largest percent difference for $\lambda = 0.53$ μm occurs for particles in the 0.5–1 fL volume range and for sphere diameter ratios near unity. Below a diameter ratio of approx. 0.75, the percent difference between comparison cases is reduced. This is expected since when the diameter ratio departs significantly from unity, the resultant bi-sphere becomes more similar to the volume equivalent sphere.

For particles with $m = 1.53 + 0i$, the largest divergence between spherical and bi-sphere geometry seem to occur for particles with sphere equivalent diameters larger than approx. Dp = 600 nm. To examine how partitioning into bi-spheres would affect integrated aerosol optical properties such as scattering or absorption coefficient, we have reconstructed aerosol scattering based on an urban aerosol size distribution reported by Zhou et al. [29]. The volume size distribution used is illustrated in Fig. 2A in blue. Also illustrated in Fig. 2A (solid red and black lines) is the size-resolved scattering coefficient reconstruction for the bi-sphere and equivalent volume sphere cases. Results suggest a slight difference of approx. 4% between the two models, with spherical geometry being higher. This analysis assumed equivalent diameter particles for the bi-sphere geometry. This shifts the optical results as far as possible from the comparison case of equivalent volume spheres, yet only a 4% difference between models results for a typical urban aerosol.

Consequently, while differences in scattering cross-section and volume scattering efficiency (ϕ_{scat}) are clearly observed, particle phase partitioning to form bi-spheres appears to affect integrated light scattering only minimally for non-light-absorbing, homogeneous particles. However, an exception to this statement would be expected for environments in which the particle size distribution deviates significantly from that used for this analysis.

Phase separation into bi-spheres may result in the two composite particles having different refractive indices. In the previous discussion, we considered bi-spheres with identical refractive index. In Fig. 2C and 2D, we consider the modeled consequences of phase separation for a second case in which the refractive index of the dielectric bi-spheres has a large difference ($m = 1.53 + 0i$; $1.35 + 0i$). These refractive index values were chosen to create a large difference in values, not to mimic any particular components of atmospheric aerosol. The plot of scattering cross-section normalized to volume (ϕ_{scat}) vs. particle volume reported in Fig. 2C appears remarkably similar to the previous case. In this case, the distribution shifts right to slightly larger particle volumes for the bi-sphere case. The percent difference between bi-sphere and volume equivalent sphere scattering cross-section (C_{scat}) is plotted in Fig. 2D as a function of total particle volume and sphere diameter ratio. The volume equivalent sphere refractive index used in the model was the volume-weighted value (e.g. $m = 1.44$ when $d_2 = d_1$). When comparing the areas shaded red (maximum difference) in Fig. 2B and 2D we see a shift towards larger volumes for the lower refractive index case. Again, the largest difference between C_{scat} consistently occurs when the bi-sphere diameter ratio is near 1. This provides strong evidence that the particle geometry is driving observed differences since it is at this sphere diameter ratio that the bi-sphere least resembles the equivalent volume sphere and the effect is refractive index independent.

Effect of bi-sphere geometry on optical properties of light-absorbing particles

Fig. 3A compares the scattering and absorption efficiencies (ϕ_{scat} and ϕ_{abs}) for bi-spheres and equivalent volume spheres for homogeneous particles with $m = 1.53 + 0.017i$. This refractive index was chosen as a rough estimate of the atmospheric aerosols' average refractive index [30–32]. As observed in Fig. 3A, the volume normalized scattering efficiency data (ϕ_{scat}) exhibited identical trend to that discussed in Section 'effect of bi-sphere geometry on scattering for homogeneous dielectric particles'. The volume normalized light absorption efficiency (ϕ_{abs}) for the bi-sphere and volume equivalent sphere cases were almost identical for the homogeneous particles. The top two plots in Fig 3A indicate differences in reconstructed light scattering and extinction between the bi-sphere and equivalent volume sphere cases for homogeneous, weakly light-absorbing particles of identical refractive index were on the order of a few percent. For both scattering and absorption, the volume equivalent sphere test case yielded slightly higher scattering and absorption coefficients (roughly 2.9% and 5% for scattering and absorption, respectively). A caveat of this analysis is the model results reflect an 'average' refractive index for atmospheric aerosol and assume a homogeneous composition for particles, however, this model is largely physically unrealistic. It is well known that different components of aerosol have varying light absorbing ability. For instance, black carbon (BC) or soot aerosol can absorb light very strongly and this aerosol component is presently thought to be insoluble and incapable of distributing itself homogeneously within particles. Furthermore, light absorbing organic molecules – here termed brown carbon (BrC), are also unlikely to partition equally between phases of a bi-phasic particle. As such, the results of Fig. 3A largely reflect a hypothetical case, rather than representative atmospheric phenomenon. However, it is interesting to note that bi-sphere geometry and volume equivalent spheres yielded nearly indistinguishable plots of ϕ_{abs} and only a 5% difference in integrated absorption for the particles considered.

The next case considered was one sphere having intermediate absorption ($m = 1.63 + 0.02i$; mimicking BrC) and the second sphere was a dielectric ($m = 1.53 + 0i$). This particular set of refractive indices were chosen to mimic mixed-phase particles containing inorganic salts and light absorbing organic compounds similar in composition to particles known as 'tarballs', brown carbon, or humic like materials [33,34]. Such bi-phasic particles could conceivably exist in the atmosphere. Fig. 3B describes the special case for when $d_1 = d_2$. Again, a shift in the ϕ_{scat} distribution for bi-spherical particles is observed relative to volume equivalent spheres. The ϕ_{abs} plots for bi-spheres and volume weighted spheres show very similar absorption efficiencies. However, if light absorption is integrated across the particle size distribution shown in Fig. 2A, a 5% difference results with the volume equivalent case resulting in slightly higher absorption.

Fig. 4 presents image plots of the percent difference in scattering and absorption cross-sections between bi-sphere and volume-weighted equivalent sphere cases for alternate scenarios. In this case, the refractive index for each sphere in the bi-sphere geometry

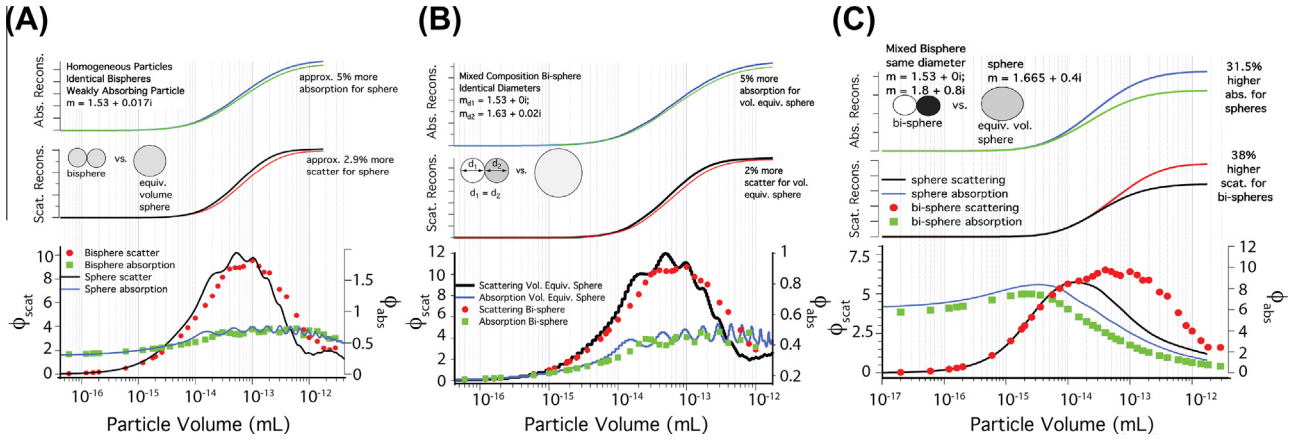

Fig. 3. Comparison of bi-spheres and equivalent volume spheres for light scattering and absorption. (A) Spheres were homogeneous and weakly light absorbing with $m = 1.53 + 0.017i$. (B) Comparison of mixed bi-sphere with volume equivalent sphere for case in which one bi-sphere exhibited weak light absorption ($m = 1.63 + 0.02i$), and the second sphere was a dielectric ($m = 1.53 + 0i$). (C) Comparison of mixed bi-sphere with volume equivalent sphere for case in which one bi-sphere was strongly light absorbing ($m = 1.8 + 0.8i$) and the second was dielectric ($m = 1.53 + 0i$). For A–C, the top two plots illustrate size-resolved, integrated light scattering and light absorption coefficients for bi-sphere and equivalent volume sphere cases. The same volume size distribution as shown in Fig 2A was used for this analysis. The bottom plot illustrates scattering and absorption efficiencies normalized to particle volume (ϕ_{scat} and ϕ_{abs}) plotted vs. particle volume.

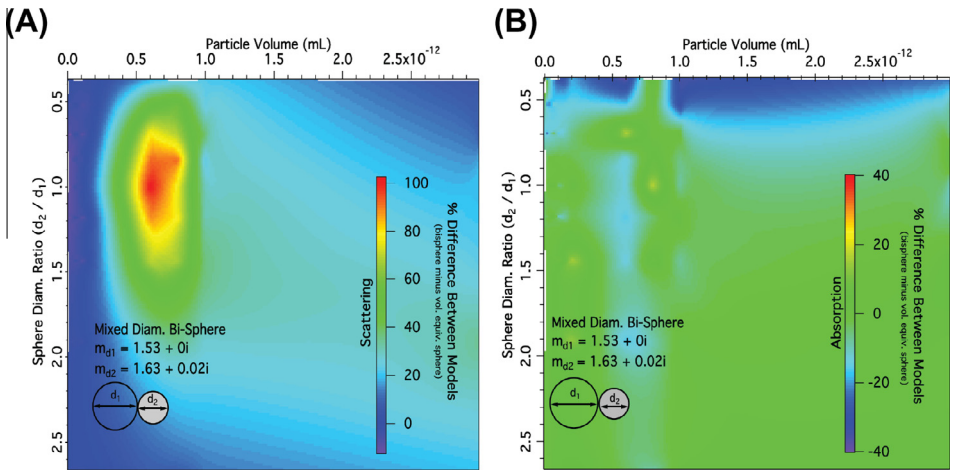

Fig. 4. Image plots of percent difference in single particle scattering (A) and absorption (B) cross-section for the bi-sphere and volume equivalent sphere test cases for a mixed bi-sphere with $m = 1.53 + 0i$ and $m = 1.63 + 0.02i$. As observed, bi-sphere arrangement of particle volume can lead to increased scattering cross-section with largest increases occurring for particles 0.5–2.0 fL and diameter ratios between 0.75 and 1.25. The observed pattern for scattering is very similar to that encountered for dielectric particles. Bi-sphere particle absorption cross-section is frequently within approx. 10–15% of the volume weighted equivalent sphere case for $d_2/d_1 > 0.5$. For smaller, light-absorbing spheres, volume-weighting leads to large over-estimates of light absorption relative to bi-spheres.

was different. One sphere was $m = 1.53 + 0i$ and the second was $m = 1.63 + 0.02i$. Results indicate scattering behavior is very similar to that which has been previously discussed. Maximum difference between C_{scat} values occur for particle volumes between 0.5 and 1 fL and a sphere diameter ratio near 1. Absorption cross-sections (C_{abs}) for the bi-sphere and volume equivalent sphere cases compare within 10–15% for most sphere diameters and particle volumes. An exception is for cases in which the absorbing particle diameter (d_2) is less than half the dielectric sphere. For such cases, the bi-sphere absorption is much less than that projected for the volume weighted equivalent sphere.

A third case considered is for one dielectric bi-sphere ($m = 1.53 + 0i$) and the second sphere a strongly absorbing particle ($m = 1.\ 8 + 0.8i$). For this case, we again compare simulated optical properties for a bi-sphere with a volume equivalent sphere. Interestingly, the light absorption efficiency (ϕ_{abs}) for the bi-sphere case was lower than the volume equivalent sphere for all particle volumes. Fig. 3C also illustrates the per-unit-volume scattering efficiency (ϕ_{scat}) extends to larger volume particles. As discussed previously, this result is very consistent among all trials, but the shift is especially pronounced for this case. Results for this case (Fig. 3C) suggest the phase separated, bi-sphere geometry leads to much higher scattering (38% higher) and lower absorption (31% less) compared to homogeneous volume equivalent spheres when integrated across the typical urban size distribution. The 31% decrease in absorption, and 38% increase in scattering are the largest changes in integrated optical properties we have observed for our comparisons of bi-spherical and volume equivalent spheres. It appears the volume-weighted equivalent sphere model does not accurately predict the optical properties of bi-sphere particles in which one sphere strongly absorbs light.

Analysis of the directionality of light scattering for bispheres

Another factor affecting climate forcing by aerosols is the angular directionality of light scattering. In the light scattering literature, angular scattering is often described by the scattering phase function. In this report, we describe angular scattering by referencing the element P_{11} of the 4×4 Mueller matrix that relates the incident and scattered Stokes parameters [35]. In addition, the angular distribution of scattering is often reduced to less detailed parameters such as asymmetry parameter (g) or backscatter fraction (b) that describe the essence of the aerosols ability to scatter in the forward or reverse direction. It should be noted that these variables refer to hemispheric scattering as referenced to the direction of an incident beam of light, and do not reflect the fraction of sunlight backscattered into space since a solar zenith angle of 0° is rarely encountered on the Earth. Values for backscatter fraction (b) and asymmetry parameter (g) can be inputted into relatively simple equations to estimate direct radiative forcing of atmospheric aerosols [36]. In general, increasing backscatter contributes to an increased aerosol cooling effect.

Fig. 5A and B illustrate image plots of the S_{11} element as a function of particle volume and scattering angle for the bi-sphere and equivalent sphere cases. Both plots appear similar with a large fraction of scattered light within the forward 20° cone. Figs. 5C and D report asymmetry parameter (g), backscatter fraction (b), and integrated backscattering considering the particle size distribution reported in Fig 2A. The plots suggest slight differences in both asymmetry parameter and backscatter fraction as a function of particle volume between the sphere and bi-sphere cases. Integration across the particle size distribution results in a 2% difference in integrated backscattering between the spherical and bi-sphere case. Modeled backscatter fractions were 0.0856 vs. 0.0873 for the two models.

Effect of core–shell geometry on scattering for dielectric particles

Fig. 6 presents plots of ϕ_{scat} and ϕ_{abs} vs. particle volume for a variety of phase separated core–shell particles. Fig. 6A reports results for a dielectric particle with a core of $m = 1.45 + 0i$ and a shell of $m = 1.53 + 0i$. The three trials reported in the plot represent three different core/particle diameter ratios ranging from 0.214 to 0.793. As observed in the plot, the red data points (core–shell model) agree very well with the solid black line (volume equivalent sphere). The largest departure between the core–shell and volume equivalent sphere models occurred at largest particle volume but was only 4.1%. Also, the value of ϕ_{scat} agreed to within 1% (core–shell vs. volume equivalent spheres) for 75% of the trials considered. This result suggests the volume-weighted averaging rule for predicting refractive index works well for non-absorbing particles provided the spherical geometry is conserved.

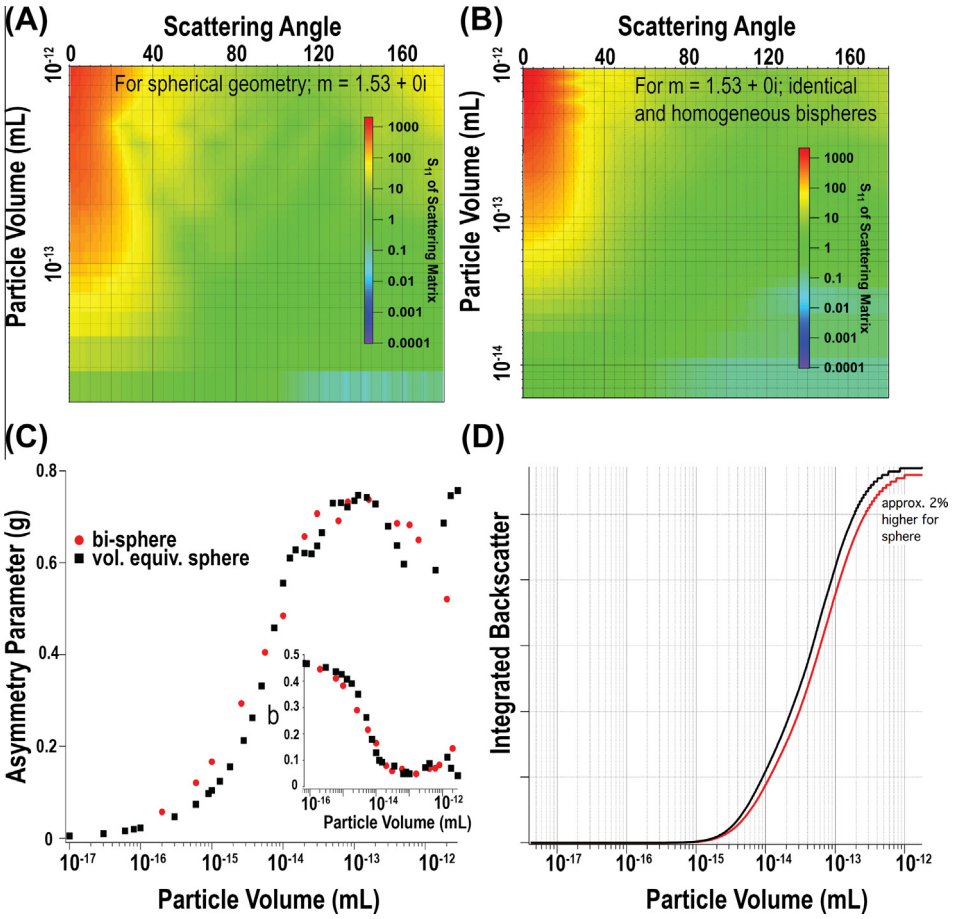

Fig. 5. (A and B) – Image plots of the S_{11} element of the scattering matrix for the spherical and bi-sphere morphology. This indicates the directionality of light scattering as a function of particle volume. Plot (C) illustrates the scattering asymmetry parameter (g) plotted vs. particle volume for the bi-sphere and equivalent sphere cases. The inset plots backscatter fraction (b) vs. particle volume. Plot (D) illustrates the integrated backscattering as reconstructed from the backscatter fraction and data in Fig. 2A. Results indicate integrated backscattering is altered by approx. 2% for the bi-sphere case.

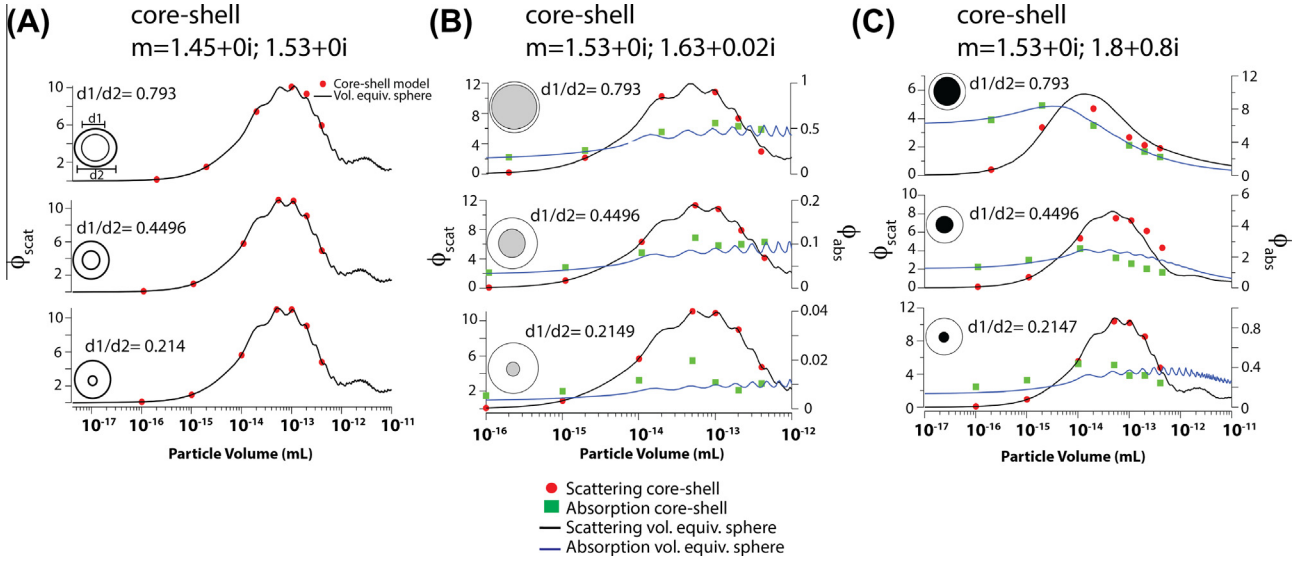

Fig. 6. Volume scattering and absorption efficiency vs. particle volume for (A) non-absorbing core–shell particles, (B) core–shell particles with weakly absorbing core, and (C) core–shell particles with a strongly absorbing core.

Effect of core–shell geometry on scattering and absorption for light absorbing particles

It has long been known that morphological alteration of light absorbing particles can influence the absorption of light by the particle. In this work, we briefly consider two cases. First, a core–shell particle with a BrC inclusion ($m = 1.63 + 0.02i$) within a shell of $m = 1.53 + 0i$. Secondly, a particle with a core of $m = 1.8 + 0.8i$ (similar to black carbon or soot) and a shell of $m = 1.53 + 0i$. Results for each are reported in Fig. 6B and C, respectively. Note, multiple core/particle diameter ratios have been considered.

For the BrC inclusion in Fig. 6B, note the good agreement between the red data points and black solid lines. These data series represent the values of ϕ_{scat} for the core–shell and equivalent sphere cases. For this case, the core–shell model and the volume-mixing model for an equivalent sphere agreed to within 1% in half of trials conducted. Maximum difference in volume scattering efficiency observed was approx. 18%. This performance remains impressive, but is slightly less effective than for dielectric particles considered in section 'effect of core-shell geometry on scattering for dielectric particles'. Results for absorption of light (illustrated on second y-axis in Fig. 6B, C) were more varied. In general, computations predicted a weakly absorbing particle core ($m = 1.63 + 0.02i$) can lead to increased volume absorption efficiency (ϕ_{abs}) relative to a homogeneously mixed volume-equivalent sphere comparison case. Similar to the case for soot inclusions, enhancements tend to be largest when the light-absorbing core has a small diameter and the shell is larger. It is not clear if such a particle morphology or absorption enhancement actually occurs for authentic aerosols containing BrC. The average difference in ϕ_{abs} between models was 24% for Fig. 6B with a maximum difference of 115%. Clearly, use of the volume-weighted mixing rule to predict light absorption by the phase-separated particles considered here is not a particularly accurate option.

Fig. 6C expands this work by considering a core–shell particle in which the core is strongly light absorbing ($m = 1.8 + 0.8i$). For the test case in which the core was nearly 80% of the outer shell diameter, the light absorption between models was close – differing by only 3.4% on average. However, for smaller cores the agreement between models was not good. The computations suggest the core–shell configuration could either increase or decrease ϕ_{abs} relative to the volume-equivalent sphere case. For small volume particles, the core–shell model often led to increases in volume absorption efficiency. For particles greater than 5×10^{-14} mL, the opposite was generally true, and the hypothetical generation of a homogeneous, fully mixed particle (e.g. use of volume equivalent sphere) led to higher volume absorption efficiency. In any event, differences between models were routinely as high as 50%. Again, this indicates the volume-weighted mixing rule does not perform well for prediction of light absorption for mixed phase particles. This is particularly true when the absorbing inclusion absorbs light strongly.

Effect of engulfed particle morphology on light scattering and absorption

We consider two distinct categories of engulfed particles, mostly engulfed and partially engulfed (consult Fig. 1). We model the mostly engulfed geometry as a two-sphere system in which the inner sphere touches the particle's edge. Fig. 7A–C reports results of the study for the mostly engulfed particles. As observed, values of ϕ_{scat} for the engulfed spheres and volume equivalent spheres agree reasonably well for all diameter ratios and refractive indices considered. Again, non-absorbing particles produced the best agreement between mostly engulfed and volume-averaged models with >80% of the ϕ_{scat} results agreeing to within 1%. Roughly 50% of the weakly absorbing particles tested exhibited ϕ_{scat} values within 1% when mostly engulfed and volume equivalent structures were compared. Larger volume particles typically exhibited larger differences between models. Differences as high as 14.2% between modeled ϕ_{scat} values were encountered for the weak light absorption case ($m = 1.53 + 0i$; $1.63 + 0.02i$). When the inclusion exhibited stronger light absorption ($m = 1.53 + 0i$; $1.8 + 0.8i$), the % difference in ϕ_{scat} between the mostly engulfed and volume equivalent models was as high as 53% with only approx. 25% of particles agreeing to within 1%.

When considering absorption of light for the mostly engulfed case with a weakly absorbing inclusion ($m = 1.63 + 0.02i$), the discrete – dipole results and volume equivalent results (ϕ_{abs}) agree to within 20% in all cases. The average discrepancy between models was 6.3%. When the inclusion was strongly absorbing, the agreement between the two cases was considerably worse. Differences in ϕ_{abs} between the models were at least 20% in nearly half of the trials considered. On occasion the percent difference reached 50%. This result also suggests using the volume-mixing rule is not accurate for particles with strongly light absorbing inclusions.

The second type of engulfed particle considered is the partially engulfed case. This particle type was largely inspired by the work of Kwamena et al. who found mixed phase particles may organize themselves by forming a thin lens or layer of organic on the surface of another material [2]. For this work, we modeled the primary sphere material as having a refractive index similar to ammonium sulfate ($m = 1.53 + 0i$). The 'lens' was modeled by creating a second sphere of varying diameter, with the sphere center offset by 25% of the first sphere's diameter. As observed in Fig. 8A, values of ϕ_{scat} for the volume-equivalent and partially engulfed models agreed to within 5% for the non-absorbing particles considered. When the 'lens' contained a weak absorber ($m = 1.62 + 0.02i$) as in Fig. 8B, similar agreement between models was observed for ϕ_{scat} (agreement to within 3.3% on average). For a weakly absorbing inclusion, the volume-weighted, partially engulfed, and mostly engulfed models yielded similar values of volume absorption efficiencies (ϕ_{abs}). The ϕ_{abs} values agreed to within 7% on average. However, when a strongly absorbing inclusion was considered for the partially engulfed morphology (as in Fig 8c), large differences between the volume weighted and engulfed models emerged. Such differences often exceeded 50%, which suggests volume averaging refractive indices is not effective when strongly absorbing inclusions are present. Significant differences in light absorption for the dark inclusion compared to the volume averaged case was observed for all models.

Conclusions & limitations of the analysis

Results suggest that distributing aerosol volume as phase separated bi-spheres can, in principle, significantly alter light scattering and absorption cross-sections and scattering and absorption efficiencies (ϕ_{scat} and ϕ_{abs}) for individual particles. Plots of volume normalized scattering efficiency (ϕ_{scat}) vs. single particle volume for the bi-sphere geometry were often shifted to larger volumes when compared to volume equivalent spheres. This effect was observed regardless of particle refractive index, indicating the particle shape was the driving force behind the effect. However, when an urban size distribution was used to model the expected integrated scattering coefficient (m^{-1}), results suggest the bi-sphere and equivalent sphere models agree to within approx. 10% for non-absorbing or weakly absorbing particles. Since the model assumed every particle was distributed as a bi-sphere, and this is likely an unrealistic assumption, the modeled result suggests phase partitioning into bi-spheres may cause only a minor alteration of integrated scattering for non-absorbing or weakly

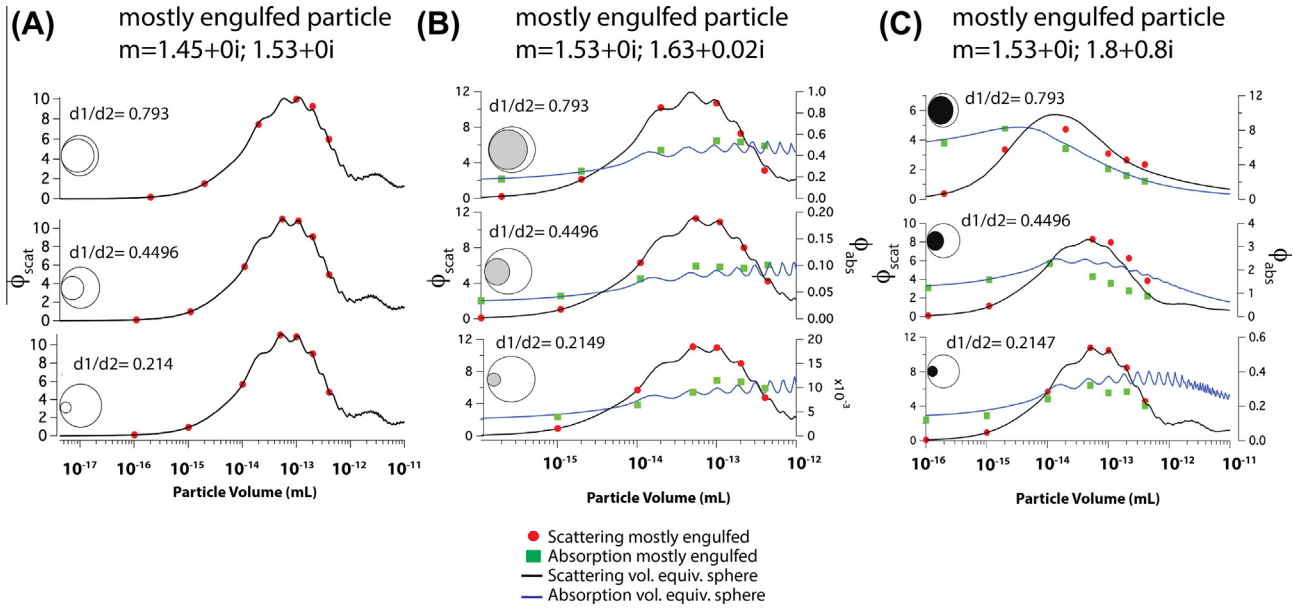

Fig. 7. Volume scattering and absorption efficiency vs. particle volume for (A) non-absorbing mostly engulfed particles, (B) mostly engulfed particles with weakly absorbing core, and (C) mostly engulfed particles with a strongly absorbing core.

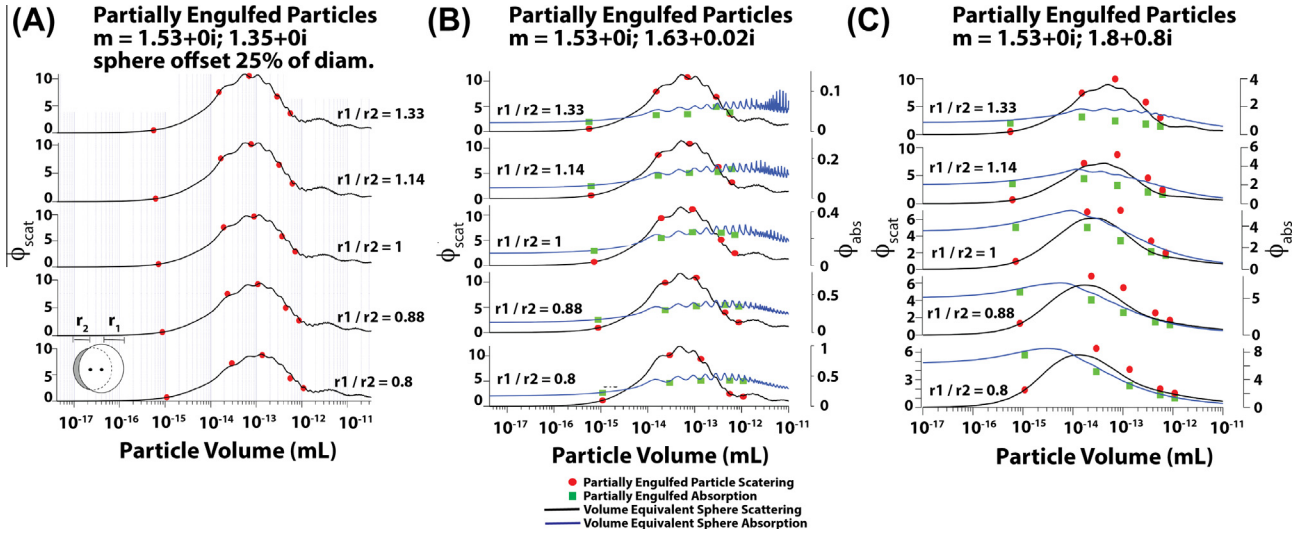

Fig. 8. Plots of volume scattering and absorption efficiency vs. particle volume for (A) non-absorbing particles, (B) weakly absorbing particles, and (C) particles with a strongly absorbing surface inclusion or shell. Case A mimics an organic shell or lens containing a non-absorber. Case B mimics an organic lens containing weakly absorbing BrC.

absorbing atmospheric aerosols. This may explain why reconstruction of aerosol scattering through use of size-distributions and assumption of spherical geometry has been successfully described in the literature [37–39].

We also determined that phase separated bi-spheres, and engulfed particles absorb light similarly (<10–15% difference) to their volume equivalent counterpart spheres for weakly light absorbing particles resembling properties of atmospheric brown carbon, humic-like materials, or tarballs. However, for a bi-sphere with one strongly light – absorbing sphere, both absorption cross-sections and integrated light absorption can be >30% different from the volume equivalent sphere case. Similar magnitude errors were found when considering dark inclusions within engulfed and core–shell particles.

In terms of broader science implications, this effort and the previous experimental work of Lang-Yona et al. [17] provide significant insights into the applicability of the linear volume-mixing based approach for prediction of refractive index for internally mixed aerosol. Our results suggest that prediction of refractive index of internally mixed particles via using volume-mixing ratios is frequently very accurate for non-absorbing or very weakly absorbing particles of near spherical morphology. However, for particles that have strongly absorbing inclusions the volume mixing approach frequently predicts absorption very different from the explicit and exact models of particles. Results of this study are largely consistent with the previous experimental observations. For instance, Lang Yona et al. found linear volume mixing rules could be used to predict refractive index/optical behavior of non-absorbing and very weakly absorbing particles. However, when the authors attempted to apply the same rules to strongly light absorbing particles, significant errors resulted [40]. Both the previous experimental results and this computational effort

suggest linear volume mixing rules are often inaccurate for modeling light absorption by aerosols.

In addition, we report that partitioning particles into bi-sphere geometry does not radically affect asymmetry parameter (g) or backscatter fraction (b) when considering integrated light scattering across the particle size-distribution. This result suggests considering bi-sphere morphology effects may not be necessary to effectively model backscattering and climate forcing by aerosol particles. Such a realization is significant to climate modeling efforts since it eliminates computational resources that otherwise might be required to model atmospheric radiative transport. Since the bi-sphere geometry is furthest removed from the volume equivalent sphere case, it is safe to assume the core–shell or engulfed geometries will not produce backscatter fractions vastly different from volume equivalent spheres.

Also, we have given descriptive statistics in terms of % difference between models, or the fraction of runs agreeing to within a certain percent. We intend these values to be quantitative guides for the reader of the general agreement between models. These values will change depending on the situational specifics, and the statistical values given are not intended to serve as bounds or limits to the accuracy of the linear volume mixing rule.

This work considers only the morphological differences of particle organization. If bi-sphere, core–shell or engulfed geometry leads to alteration of chemical processes leading to increases or decreases in aerosol mass yields or prevalence, this would not be accounted for in this analysis. In fact, any secondary effect of the bi-sphere relative to the volume equivalent sphere is not considered here. Furthermore, particle size also appears to be an important factor affecting phase separation as Veghte et al. [3] found mixed phase particles below approx. Dp = 200 nm tend to be homogeneous, however larger particles of pimelic or succinic acid mixed with ammonium sulfate readily phase separated. No such effects are considered here.

References

[1] You Y, Renbaum-Wolff L, Carreras-Sospedra M, Hanna SJ, Hiranuma N, Kamal S, Smith ML, Zhang X, Weber R, Shilling JE, Dabdub D, Martin ST, Bertram A. Images reveal that atmospheric particles can undergo liquid–liquid phase separations. Proc Natl Acad Sci USA 2012;109:13188–93.

[2] Kwamena N-OA, Buajarern J, Reid JP. Equilibrium morphology of mixed organic/inorganic/aqueous aerosol droplets: investigating the effect of relative humidity. J Phys Chem A 2010;114(18):5787–95.

[3] Veghte DP, Bittner DR, Freedman MA. Cryo-transmission electron microscopy imaging of the morphology of submicrometer aerosol containing organic acids and ammonium sulfate. Anal Chem 2014;86(5):2436–42.

[4] Veghte DP, Bilal Altaf M, Freedman MA. Size dependence of the structure of organic aerosol. J Am Chem Soc 2013;135(43):16046–9.

[5] Song M, Marcolli C, Krieger UK, Zuend A, Peter T. Liquid–liquid phase separation in aerosol particles: Dependence on O:C, organic functionalities, and compositional complexity. Geophys Res Lett 2012;39:L19801. http://dx.doi.org/10.1029/2012GL052807.

[6] Ciobanu VG, Marcolli C, Krieger UK, Weers U, Peter T. Liquid−liquid phase separation in mixed organic/inorganic aerosol particles. J Phys Chem A 2009;113(41):10966–78.

[7] You Y, Renbaum-Wolff L, Bertram AK. Liquid–liquid phase separation in particles containing organics mixed with ammonium sulfate, ammonium bisulfate, ammonium nitrate or sodium chloride. Atmos Chem Phys 2013;13:11723–34.

[8] Thompson JE, Spangler H. Tungsten source integrated cavity output spectroscopy (W-ICOS) for the determination of ambient atmospheric extinction coefficient. Appl Opt 2006;45(11):2465–73.

[9] Thompson JE, Barta N, Policarpio D, DuVall R. Development of a fixed frequency aerosol albedometer. Opt Express 2008;16(3):2191–205.

[10] Redmond H, Dial K, Thompson JE. Light scattering & absorption by wind blown dust: theory, measurement and recent data. Aeolian Res 2010;2:5–26.

[11] Dial K, Hiemstra S, Thompson JE. Simultaneous measurement of optical scattering and extinction on dispersed aerosol samples. Anal Chem 2010;82:7885–96.

[12] Redmond H, Thompson JE. Evaluation of a quantitative structure property relationship (QSPR) for predicting mid-visible refractive index of secondary organic aerosol (SOA). Phys Chem Chem Phys 2011;13:6872–82.

[13] Thompson JE, Hayes PL, Jimenez JL, Adachi K, Zhang X, Liu J, Weber RJ, Buseck PR. Aerosol optical properties at Pasadena, CA during CALNEX 2010. Atmos Environ 2012;55:190–200.

[14] Ma L, Thompson JE. Optical properties of dispersed aerosols in the near UV (355 nm): measurement approach and initial data. Anal Chem 2012;84(13):5611–7.

[15] Wei Y, Ma L, Cao T, Zhang Q, Wu J, Buseck PR, Thompson JE. Light scattering and extinction measurements combined with laser-induced incandescence for the real-time determination of soot mass absorption cross section. Anal Chem 2013;85(19):9181–8.

[16] Wei Y, Zhang Q, Thompson JE. Atmospheric black carbon can exhibit enhanced light absorption at high relative humidity. Atmos Chem Phys Discuss 2013;13:29413–45.

[17] Lang-Yona N, Abo-Riziq A, Erlick C, Segre E, Trainic M, Rudich Y. Interaction of internally mixed aerosols with light. Phys Chem Chem Phys 2010;12:21–31.

[18] Yurkin MA, Hoekstra AG. The discrete-dipole-approximation code ADDA: capabilities and known limitations. J Quant Spectrosc Radiat 2011;112:2234–47.

[19] Flatau PJ, Fuller KA, Mackowski DW. Scattering by two spheres in contact: comparisons between discrete-dipole approximation and modal analysis. Appl Opt 1993;32(18):3302–5.

[20] Xu Y, Gustafson BAS. Comparison between multisphere light-scattering calculations: rigorous solution and discrete-dipole approximation. Astrophys J 1999;513:894–909.

[21] Chylek P, Videen G, Gel dart DJW, Dobbie JS, Tso HCW. Effective medium approximations for heterogeneous particles in: light scattering by nonspherical particles, theory, measurements and application. Academic Press; 2000.

[22] Jacobson MZ. Effects of externally-through-internally-mixed soot inclusions within clouds and precipitation on global climate. J Phys Chem A 2006;110:6860–73.

[23] Stelson AW. Urban aerosol refractive index prediction by partial molar refraction approach. Environ Sci Technol 1990;24:1676–9.

[24] Chylek P, Ramaswamy V, Cheng RJ. Effect of graphitic carbon on the albedo of clouds. J Atmos Sci 1984;41:3076–84.

[25] Burton SP, Vaughan MA, Ferrare RA, Hostetler CA. Separating mixtures of aerosol types in airborne high spectral resolution lidar data. Atmos Meas Tech 2014;7:419–36. http://dx.doi.org/10.5194/amt-7-419-2014.

[26] Bohren CF, Huffman DR. Absorption and scattering of light by small particles. Wiley VCH; 2004. ISBN 0-471-29340-7.

[27] Marshall SF, Covert DS, Charlson RJ. Relationship between asymmetry parameter and hemispheric backscatter ratio: implications for climate forcing by aerosols. Appl. Opt. 1995;34(27):6306–11.

[28] Um J, McFarquhar GM. Optimal numerical methods for determining the orientation averages of single-scattering properties of atmospheric ice crystals. J Quant Spectrosc Radiat Transfer 2013;127:207–23.

[29] Zhou L, Kim E, Hopke PK, Stanier CD, Pandis S. Advanced factor analysis on Pittsburgh particle size-distribution data. Aerosol Sci Technol 2004;38(S1):118–32.

[30] Levoni C, Cervino M, Guzzi R, Torricella F. Atmospheric aerosol optical properties: a database of radiative characteristics for different components and classes. Appl Opt 1997;36(30):8031–41.

[31] Pandithurai G, Devara PCS, Ernest Raj P, Sharma S. Aerosol size distribution and refractive index from bistatic lidar angular scattering measurements in the surface layer. Remote Sens Environ 1996;56:87–96.

[32] Kocifaj M, Horvath H, Jovanović O, Gangl M. Optical properties of urban aerosols in the region Bratislava-Vienna I. Methods and tests. Atmos Environ 2006;40:1922–34.

[33] Adachi K, Buseck PR. Atmospheric tar balls from biomass burning in Mexico. J Geophys Res 2011;116:D05204. http://dx.doi.org/10.1029/2010JD015102.

[34] Pósfai M, Gelencsér A, Simonics R, Arató K, Li J, Hobbs PV, Buseck PR. Atmospheric tar balls: particles from biomass and biofuel burning. J Geophys Res 2004;109:D06213. http://dx.doi.org/10.1029/2003JD004169.

[35] Yang P, Bi L, Baum BA, Liou KN, Kattawar GW, Mishchenko MI, Cole B. Spectrally consistent scattering, absorption, and polarization properties of atmospheric ice crystals at wavelengths from 0.2 to 100 μm. J Atmos Sci 2013;70:330–47.

[36] Haywood JM, Shine KP. The effect of anthropogenic sulfate and soot aerosol on the clear sky planetary radiation budget. Geophys Res Lett 1995;22:603–6.

[37] Sciare J, Oikonomou K, Cachier H, Mihalopoulos N, Andreae MO, Maenhaut W, Sarda-Estève R. Aerosol mass closure and reconstruction of the light scattering coefficient over the Eastern Mediterranean Sea during the MINOS campaign. Atmos Chem Phys 2005;5:2253–65. http://dx.doi.org/10.5194/acp-5-2253-2005.

[38] Highwood EJ, Northway MJ, McMeeking GR, Morgan WT, Liu D, Osborne S, Bower K, Coe H, Ryder C, Williams P. Aerosol scattering and absorption during the EUCAARI-LONGREX flights of the facility for airborne atmospheric measurements (FAAM) BAe-146: can measurements and models agree? Atmos Chem Phys 2012;12:7251–67. http://dx.doi.org/10.5194/acp-12-7251-2012.

[39] <http://vista.cira.colostate.edu/improve/tools/reconbext/reconbext.htm>; [accessed March 31 2014].

[40] Abo Riziq A, Erlick C, Dinar E, Rudich Y. Optical properties of absorbing and non-absorbing aerosols retrieved by cavity ring down (CRD) spectroscopy. Atmos Chem Phys 2007;7:1523–36. http://dx.doi.org/10.5194/acp-7-1523-2007.